Electrochimica Acta 477 (2024) 143771

Contents lists available at ScienceDirect

Electrochimica Acta

journal homepage: www.journals.elsevier.com/electrochimica-acta

Investigating the V(II)/V(III) electrode reaction in a vanadium redox flow battery – A distribution of relaxation times analysis

Monja Schilling [a], Roswitha Zeis [a,b,c,*]

[a] Karlsruhe Institute of Technology, Helmholtz Institute Ulm, Helmholtzstraße 11, D-89081 Ulm, Germany
[b] Department of Electrical, Electronics, and Communication Engineering, Faculty of Engineering, Friedrich-Alexander-Universität Erlangen-Nürnberg (FAU), Cauerstraße 9, Erlangen 91058, Germany
[c] Department of Mechanical & Industrial Engineering, Faculty of Applied Science & Engineering, University of Toronto, 5 King's College Road, Toronto, Ontario M5S 3G8, Canada

ARTICLE INFO

Keywords:
Vanadium redox flow battery
Flow cell
Electrochemical impedance spectroscopy (EIS)
Distribution of relaxation times (DRT)
V(II)/V(III) redox reaction

ABSTRACT

Vanadium Redox Flow Batteries (VRFBs) are already commercially available and promise to provide excellent prerequisites to face the challenge of large-scale energy storage. Nevertheless, the VRFB itself has to overcome challenges regarding lifetime and efficiency. Polarization and pumping losses due to a high electrolyte flow-through resistance in the electrode contribute to much of the efficiency losses. We investigated the reaction and processes in the negative VRFB half-cell using electrochemical impedance spectroscopy combined with the distribution of relaxation times analysis. We identify the individual processes in the negative half-cell by varying several parameters. One peak is observed in the low-frequency range below 2 mHz, attributed to the ion transport. In the range from 2 mHz to 1 Hz, several peaks are identified and assigned to the redox-active species' transport processes through the electrode's porous structure. In the high-frequency range above 1 Hz, the single peak was assigned to the electrochemical reaction in the negative half-cell. The processes in this half-cell are slower than in the positive half-cell. The technique is beneficial to gain a fundamental understanding of the catalytic process of the V(II)/V(III) reaction to optimize novel electrode materials or monitor electrode degradation processes.

1. Introduction

The Vanadium Redox Flow Battery (VRFB), developed in the 1980s by the group of Skyllas-Kazacos [1], is a promising candidate for large-scale energy storage to balance the fluctuations of renewable energy sources [2]. VRFBs are already commercially available but face significant lifetime and efficiency challenges. Polarization and pumping losses due to the high flow-through resistance of the electrolyte in the electrode account for a large part of the efficiency losses [3,4]. Furthermore, the efficiency is reduced by the degradation of the electrode [5–8], the solubility of the active vanadium species in the electrolyte [9], ion crossover [10], and side reactions such as the hydrogen evolution in the negative half-cell [11–14].

The electrode material must be highly catalytically active towards the desired vanadium reaction and prevent side reactions such as hydrogen evolution reaction (HER) to ensure excellent performance of the VRFB. Studying the reaction mechanism in the half-cells can be beneficial to evaluate electrode material for VRFBs. Investigating this reaction type is challenging because of electrolyte stability issues and the HER at the same potential range. A stable measurement signal is crucial for electrochemical techniques such as cyclic voltammetry or Electrochemical Impedance Spectroscopy (EIS). Due to the formation of hydrogen bubbles as an undesired side reaction, the signal is often noisy and does not allow proper characterization. Nevertheless, many research groups worldwide investigated the reaction mechanism in the negative half-cell, and several mechanisms have been proposed [15–22]. These studies state that the reaction pathway most likely occurs via an inner-sphere mechanism, and oxygen-containing functional groups are beneficial since the vanadium ions adsorb at these active sites during the oxidation or reduction reaction between V(II) and V(III). Thus, the transport and diffusion of the vanadium species to the active sites on the electrode material must play an important role.

* Corresponding author at: Faculty of Engineering, Department of Electrical, Electronics, and Communication Engineering, Friedrich-Alexander-University Erlangen-Nürnberg (FAU), Cauerstraße 9, Erlangen 91058, Germany.
E-mail address: roswitha.zeis@fau.de (R. Zeis).

https://doi.org/10.1016/j.electacta.2024.143771
Received 26 October 2023; Received in revised form 8 December 2023; Accepted 2 January 2024
Available online 3 January 2024

Furthermore, more insights into the cell losses, including kinetic, ohmic, and transport losses, are crucial for improving the electrode materials for VRFBs and optimizing their performance. EIS can characterize the cell losses *in situ* and resolve the processes occurring on different time scales [23–26]. For VRFBs, the flow cell setup developed by Schilling et al. enables EIS measurements of a half-cell under application-oriented conditions [27]. EIS data are often analyzed using an equivalent circuit model [28–30]. In the case of superimposed signals, identifying an appropriate equivalent circuit model can be very challenging without prior knowledge about the system. In previous studies [6,25,27,31], we demonstrated that EIS combined with the Distribution of Relaxation Times (DRT) analysis could be successfully applied to analyze the performance of high-temperature PEM fuel cells, vanadium redox flow batteries, and electrochemical hydrogen pumps. They decomposed the polarization losses of the electrochemical cell based on their typical time constants. The main features of their distribution functions could be assigned to individual cell processes, such as electrode reaction kinetics and gas and ion transport phenomena, by selecting appropriate experimental conditions. Therefore, we developed a novel flow cell to study the processes in a VRFB half-cell under controlled operating conditions. In the positive half-cell, processes in three different frequency ranges were identified, corresponding to the electrochemical reaction, the transport processes through the porous structure of the electrode, and the ion transport [27]. Furthermore, the flow cell setup was used to study the effects of the thermal activation of carbon felt electrodes on their wettability and the transport processes in the electrode [6]. Carbon-based materials with high transport-related impedances in the DRT analysis also exhibit a hampered electrolyte injection behavior in synchrotron X-ray imaging experiments [32,33].

In this study, we investigate the processes in the negative half-cell of a VRFB using EIS combined with the DRT analysis. Thereby, several experimental parameters are varied to investigate their influence on the individual impedances in the system. This approach allowed us to assign the peaks in the DRT spectrum to the electrochemical reaction of the active V(II)/V(III) species, the transport process through the porous structure of the electrode, and the ion transport. Furthermore, the differences between the negative and positive half-cell processes are discussed, and the different time scales of the processes are highlighted. The information gained about the reaction, the reaction mechanism, and the transport processes is beneficial for studying novel electrode materials, their optimization, and simulation work.

2. Experimental

2.1. Materials and electrolytes

The carbon felt SIGRACELL® GFA 6.0 EA (SGL Carbon, Meitingen, Germany) and the carbon paper SIGRACET® GDL 39 AA (SGL Carbon, Meitingen, Germany) were thermally pretreated as proposed in the literature to enhance their wettability and electrochemical performance [5,34]. The carbon materials were placed in a covered glass petri dish and heated to 400 °C for 25 h in a muffle furnace in an air atmosphere. The carbon materials were immersed in ultrapure water (18.2 MΩ cm) and sonicated for two minutes to remove contaminations and small fiber fragments from cutting before assembling the cell.

V(IV) electrolyte was prepared by dissolving $VOSO_4$ (vanadyl sulfate hydrate, 99.9 % metal basis, Thermo Fisher Scientific) in diluted H_2SO_4 (diluted from concentrated sulfuric acid, 96 %, Suprapur®, Merck with ultrapure water (18.2 MΩ cm)) to obtain 0.1 M $VOSO_4$ in 2 M H_2SO_4.

Starting from the V(IV) electrolyte, a charging procedure was performed to receive the V(II) electrolyte using a VRFB in a redox flow test system (Scribner 857 Redox Flow Cell Test System, Scribner Associates Inc.). First, a constant current of 40 mA cm^{-2} was applied until a cut-off cell voltage of 1.8 V was reached. Second, a constant cell voltage of 1.8 V was applied until the current was lower than 1 mA cm^{-2}.

To obtain electrolytes with an SoC other than 0 % or 100 %, V(II) and V(III) electrolytes were mixed in the appropriate ratio.

2.2. Experimental setup

The electrochemical measurements were performed with an in-house developed, 3D-printed flow cell designed to ensure steady-state conditions during the experiment and mimic a commercial VRFB's behavior. A detailed cell description is available in Schilling et al.'s previous publication [27], and a schematic drawing is given in Fig. S1 in the supporting information. In short, a piece of carbon material (1.0 cm x 1.0 cm) was placed in the flow channel of the flow cell as the working electrode (WE) and was contacted with a 1.0 mm thick titanium foil (99.2 % Alfa Aesar). As a counter electrode (CE), three pieces of carbon paper were stacked on each other and contacted with titanium foil. Both titanium foils were electrically contacted with a titanium wire (0.28 mm diameter, Alfa Aesar). A stack of five pieces of carbon paper was used as the WE, whereas a single piece was used for the carbon felt. An in-house developed hydrogen reference electrode was inserted as the reference electrode (RE).

The EIS measurements were performed with the setup displayed in Fig. 1. The flow cell is combined with a VRFB full cell to ensure that the electrolyte is always fully charged during the measurements since the SoC influences the EIS spectrum [27]. The anolyte is pumped from the reservoir (Fig. 1, bottom left) to the VRFB full cell, where it is charged at a constant cell potential of 1.8 V and then pumped to the second reservoir (Fig. 1, top left). All electrolyte reservoirs were kept under a nitrogen atmosphere. Next, the electrolyte is pumped from this reservoir through the flow cell for the EIS measurement and back to the same reservoir. Finally, the electrolyte is pumped from this reservoir to the original anolyte reservoir (bottom left) to complete the charging and measuring cycle. Peristaltic pumps (Masterflex L/S®, Cole-Parmer) were used to transport the electrolyte through the setup. For experiments at elevated temperatures, the electrolyte reservoir connected to the flow cell was placed in an oil bath, and the measurement was started after an equilibration period of 1.5 h. The catholyte reservoir contains the electrolyte used in the positive half-cell during the charging process, continuously circulating between the VRFB cell and the reservoir.

2.3. Electrochemical impedance spectroscopy and data processing

The electrochemical measurements were performed in the described setup using an SP-300 potentiostat (BioLogic Science Instruments). The following parameters were varied independently: the carbon material used as the WE, the flow rate, the concentration of the vanadium species, the temperature, the applied WE potential, and the SoC of the electrolyte. When not noted otherwise, the standard conditions were applied:

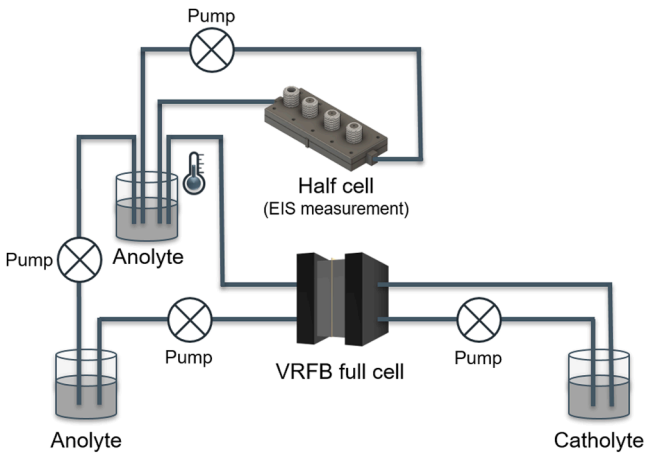

Fig. 1. The experimental setup scheme combines the flow cell for the EIS measurements with a VRFB full cell used to charge the electrolyte.

room temperature, carbon paper as the WE and the CE, flow rate of 15 mL min^{-1}, standard electrolyte with 0.1 M V(II) in 2 M sulfuric acid, WE potential of –0.30 V vs. RHE. The measurements were performed in the potentiostatic mode in a frequency range from 100 kHz to 3.5 mHz with a single sinusoidal excitation of 10 mV as the perturbation.

The Kramers-Kronig transform evaluated the data quality according to the standard procedure provided by Schönleber et al. [35,36]. The data were further analyzed using the MATLAB-based tool DRTtools [37] based on the Tikhonov regularization. The spectra fitting is based on a Gaussian function for the discretization and includes the inductive data. As a regularization parameter, 1E-9 was chosen.

3. Results and discussion

Herein, we first propose the assignments of the DRT peaks from EIS measurements in the negative half-cell of a VRFB. These assignments were made by varying parameters and studying their influence on the DRT spectrum. Second, the results from the parameter variations are displayed and discussed in detail in the subsequent sub-sections.

3.1. Peak assignments of the drt spectra

We used the DRT analysis to obtain DRT spectra of the EIS measurements in the negative half-cell of a VRFB. The peaks in the DRT spectra are related to the occurring processes, and a frequency can be assigned to each process. Fig. 2 presents an exemplary DRT spectrum of the negative half-cell with the distribution function of the relaxation times g(f) plotted against the frequency f. By the variation of different experimental parameters, three characteristic frequency ranges were identified in the DRT spectrum, highlighted in different colors. One peak was observed in the high-frequency (HF) range above 1 Hz (highlighted in yellow). This peak corresponds to the electrochemical redox reaction of the active redox couple V(II)/V(III). Several peaks are observed in the mid-frequency (MF) range between 1 Hz and 2 mHz (highlighted in green). These peaks are assigned to transport the redox-active species in the electrolyte through the porous electrode structure. The low-frequency (LF) range below 2 mHz (highlighted in blue) displays one single peak also assigned to a transport-related process –ion transport.

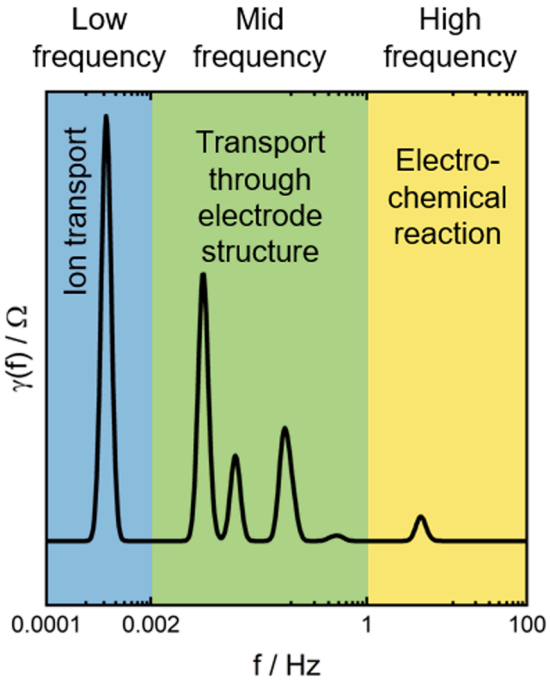

Fig. 2. Exemplary DRT spectrum of the negative VRFB half-cell with the respective frequency ranges and peak assignments to the occurring processes.

We observed a slight shift of the single peak in the low-frequency range when using different carbon-based electrode materials as the WE. The assignments and frequencies displayed herein are valid for carbon paper as the WE material. In the case of carbon felt, the peak in the low-frequency range shifts to slightly higher frequencies. Similar observations were previously reported in the literature [6].

We assigned the peaks in the DRT spectrum to the same processes reported for the positive half-cell [27]. However, the peak frequencies are severely shifted since the processes in the negative half-cell are generally slower. Therefore, the respective frequency ranges related to the electrochemical reaction, electrolyte transport through the porous electrode structure, and ion transport were adapted accordingly and appeared at lower frequencies.

3.2. Influence of the electrode materials

Carbon paper and carbon felts are commonly used as electrode materials in VRFBs [2,21]. Here, we investigate the influence of these two materials on the DRT spectrum of the negative VRFB half-cell. Carbon felts are highly porous materials that are fabricated from graphitized fibers. The herein-used carbon felt has an open porosity of 95 % [38] and a disordered fiber arrangement. Carbon paper is manufactured from chopped fibers glued with a binder to form a thin electrode [39]. The carbon paper used in this study has an open porosity of 89 % [40]. A display of the herein-used carbon paper and carbon felt using different magnifications and techniques, including light microscopy and scanning electron microscopy, can be found in a previous publication by Schilling et al. [27]. The different morphology of both materials will influence the flow-through behavior of the electrolyte through the electrode and, therefore, the impedance and the DRT spectrum.

Fig. 3a presents Nyquist plots of the EIS measurements using the different carbon materials as the WE. The corresponding DRT spectra and the bar diagrams summarizing the contributions to the individual frequency ranges are displayed in s 3b and c, respectively. The Nyquist plots of both materials differ significantly in shape. The overall impedance is also a higher manifold for the carbon paper than the carbon felt. If carbon paper is used as the WE (Fig. 3a, grey curve), the Nyquist plot shows a small semicircle at high frequencies followed by several overlapping semicircles at lower frequencies. In the high-frequency range, a vertical line below the x-axis is observed, corresponding to the setup's inductance, including the cables and the titanium wires used to contact the electrode material electrically. This feature was observed for both materials since it only relates to the setup. By eye, it is challenging to identify the number of superimposed semicircles. However, the DRT analysis helps to face this challenge by placing the number of RC elements connected in series, which describes the respective impedance spectrum most adequately. Each RC element corresponds to one semicircle and, therefore, to one peak in the DRT spectrum. As explained in the previous section, six peaks were identified for carbon paper as the WE assigned to three frequency ranges.

The carbon felt has a much lower overall impedance than the carbon paper. The Nyquist plot consists of a straight vertical line below the x-axis, followed by an elongated superimposed semicircle and another at lower frequencies (Fig. 3a, red curve). The DRT spectrum of the carbon felt shows fewer peaks (Fig. 3b), with one single peak in the high-frequency range related to the electrochemical reaction, followed by two peaks (compared to four peaks with carbon paper) in the mid-frequency range and a single peak in the low-frequency range.

Comparing the two impedance spectra, the impedance related to the electrochemical reaction (HF range) is around three times larger for the carbon felt than the carbon paper. Since the frequency does not change, the rate-determining step seems identical. However, different active sites in the materials might explain the significant difference in the HF impedance. Carbon felt consists of graphitized carbon fibers, whereas carbon paper comprises chopped fibers and carbonized glue-containing

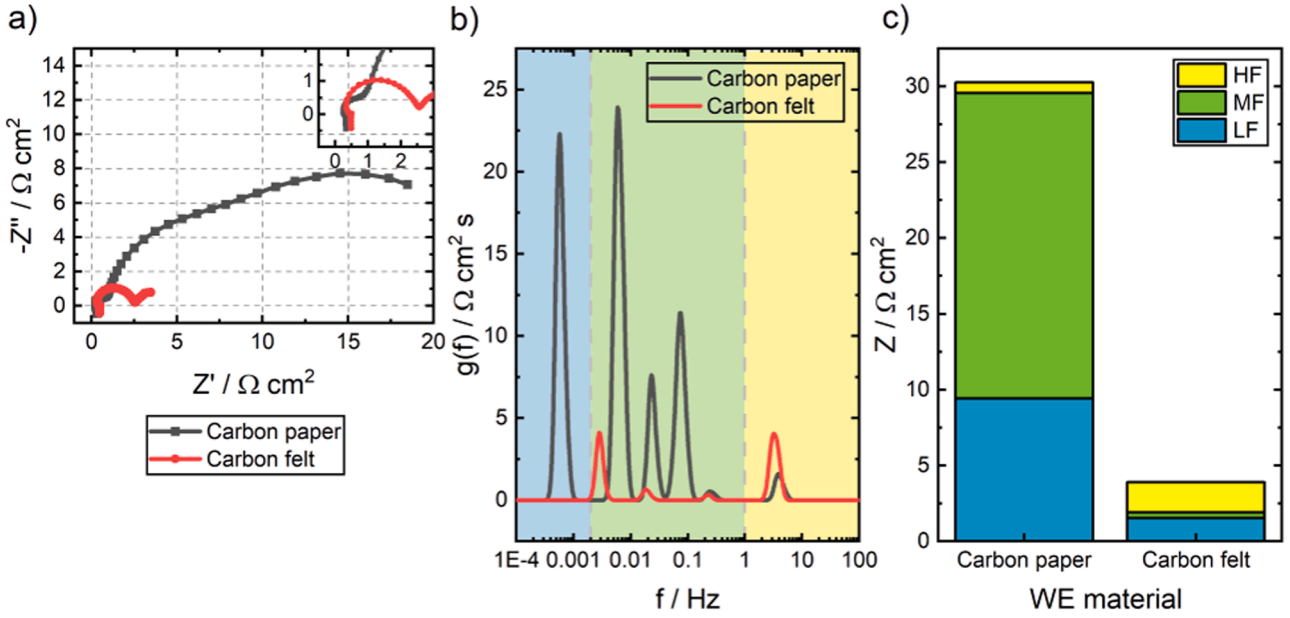

Fig. 3. (a) Nyquist plots and (b) corresponding DRT spectra using different WE materials (carbon felt or carbon paper). (c) Total impedance values contributing to the assigned frequency ranges.

binder [41]. Thus, the carbon paper surface consists of various active sites (fibers and binder). Different active sites likely have another catalytic activity towards the V(II)/V(III) reaction; therefore, a different HF impedance is observed at a similar frequency. The number of peaks and impedance values in the MF range differs significantly, showing that the morphology influences the transport process through the porous structure. Two relatively small peaks are observed for the carbon felt, whereas the measurement with carbon paper results in four peaks in this frequency range. The peak at around 0.2 Hz is identical for carbon felt and carbon paper. Thus, a similar process related to the transport through the porous structure should occur. Since only fibers are present in both materials, this process could be associated with this component. The other peaks in this frequency range are not identical and seem related to the electrode materials' unique structural features or elements. The single peak in the low frequency is shifted to higher frequencies. It has a lower impedance for the carbon felt WE, which shows that the ion transport must be facilitated compared to the carbon paper material. Since some pathways in the structure of carbon paper are blocked by the binder, higher MF and LF impedances might be explained by this hindered transport.

In the following, carbon paper will be used as the WE, except for the section about the influence of the flow rate (carbon felt: Fig. 4, carbon paper: Figure in the supporting information). Since the choice of the electrode material also influences the other parameters, a more in-depth analysis will follow in the subsequent sections.

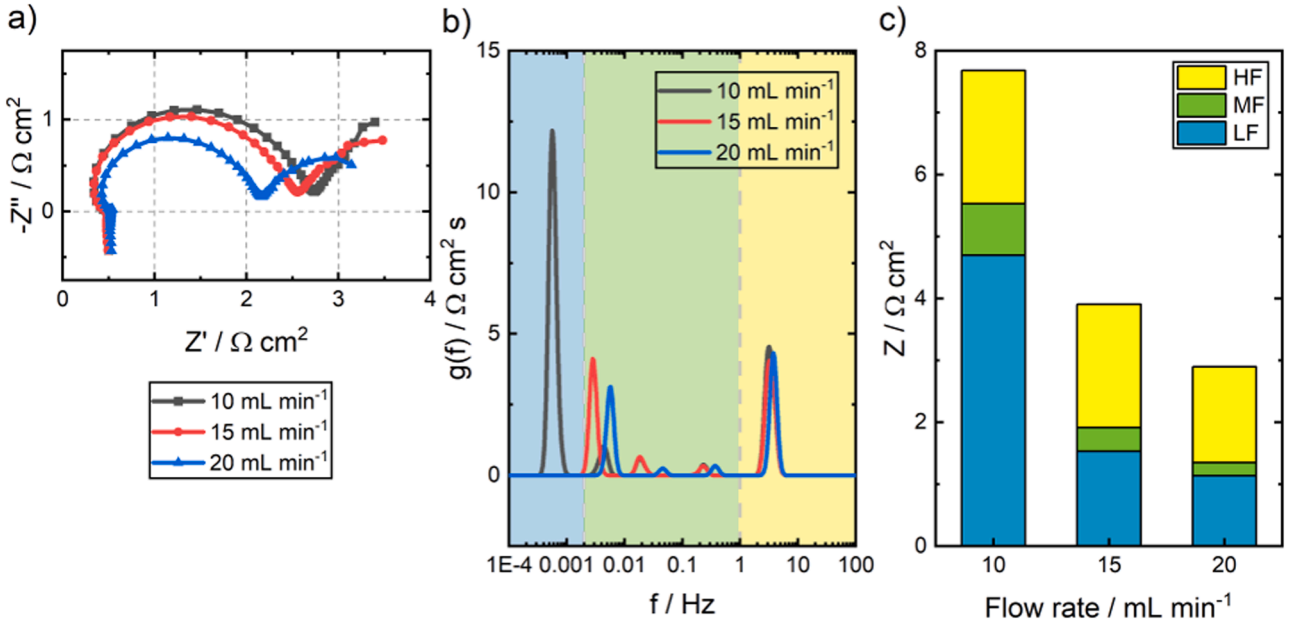

Fig. 4. (a) Nyquist plots and b) corresponding DRT spectra at different flow rates of 10, 15, and 20 mL min^{-1} using carbon felt as the WE. c) Total impedance values contributing to the assigned frequency ranges.

3.3. Influence of the flow rate

Fig. 4 displays the effect of varying the flow rate during the EIS measurements in the negative half-cell. Carbon felt was used as the WE since more significant differences in the impedance spectrum are visible for this electrode material. In the case of carbon paper as the WE, only marginal differences are observed by changing the flow rate (see supporting information, Figure).

An influence of the flow rate on the EIS measurement is already visible in the Nyquist plot (Fig. 4a). In the high-frequency range, the vertical straight line below the x-axis related to the setup is observed, similar to the previous measurements. The superimposed semicircles in the MF and the LF range get smaller at a higher flow rate. These observations can be quantified using the DRT analysis. The peak in the low-frequency range decreases with increasing flow rate (Fig. 4c) and shifts to higher frequencies simultaneously. Here, the frequency range for the LF peak was adapted for the bar diagram accordingly. The high flow rate is beneficial for the transport of vanadium ions. Thus, the impedance decreases and shifts to a higher frequency, indicating a faster and improved transport process. The same observations were made in the positive half-cell study for carbon paper and carbon felt as electrode material [27]. The flow rate affects the MF and the LF range in the negative half-cell. The transport processes in the MF range show a decreased impedance with an increasing flow rate. This effect could be caused by the increased amounts of ions transported to the electrode surface with increasing flow rate and forming a thinner double layer close to the surface. Using carbon felt as the WE, it should be noted that the impedance related to the electrochemical reaction is relatively large, and only a slight decrease of the HF impedance is observed at higher flow rates. The mechanism of the V(II)/V(III) reaction is not fully understood, and many reaction mechanisms were previously proposed in the literature, with a good overview provided by Kim et al. [21]. It could be possible that a diffusion step of the vanadium ion to the electrode's surface is the rate-limiting step. With an increasing flow rate, this process would be improved; therefore, the related impedance of the electrochemical reaction would decrease.

Overall, this experiment with different flow rates demonstrates the importance of choosing an electrode with excellent flow properties and the best corresponding flow rate for the combination of electrode and cell design. Otherwise, the efficiency of a VRFB can be significantly reduced by the losses related to the transport processes.

3.4. Influence of the V(II) concentration

Commercial VRFBs are operated at high molar concentrations of vanadium ions in the electrolyte [2,9]. Thus, we studied the influence of the V(II) concentration on the impedances of the processes in the negative half-cell. The Nyquist plots, DRT spectra, and individual impedance values are displayed in Fig. 5. At first glance, the overall impedance decreased with higher vanadium concentration. The superimposed semicircles in the Nyquist plots (Fig. 5a) corresponding to the transport-related processes are significantly reduced. Suppose a higher concentration of vanadium ions is available in the electrolyte. In that case, more vanadium ions will be closer to the electrode surface or only need to diffuse a small distance before they can react at the active site of the carbon-based material. Hence, the impedance related to the transport processes decreases. For a V(II) concentration of 0.3 M, the peak at the lowest frequency was considered the LF peak. The differences between 0.3 M and 0.5 M are minor. The V ion concentration in the electrolyte is already high. In that case, additional ions no longer affect the double layer since the increase is lower (0.1 M to 0.3 M: +200 % increase of V ions compared to 0.3 M to 0.5 M: +67 % increase of V ions). The change in viscosity due to a higher vanadium ion concentration seems to play a negligible role since the changes in viscosity should be minimal for the small changes in concentration [42].

The peak in the high-frequency range changes slightly with rising vanadium concentration. The DRT spectra (Fig. 5b) reveal that the peak frequency is unaffected; hence, the rate-determining step is the same. However, the impedance related to the HF range decreases slightly with a higher concentration of vanadium ions. The measurements from changing the flow rate indicated that the rate-determining step of the electrochemical reaction could be related to diffusion or adsorption. Both processes could be positively influenced by a higher concentration of the active species in the electrolyte, leading to a decreased HF impedance at rising concentrations. Nevertheless, the effect on the electrochemical reaction is relatively small compared to the impact on the transport-related processes. Furthermore, the reaction mechanism is investigated by many research groups, and many different pathways are

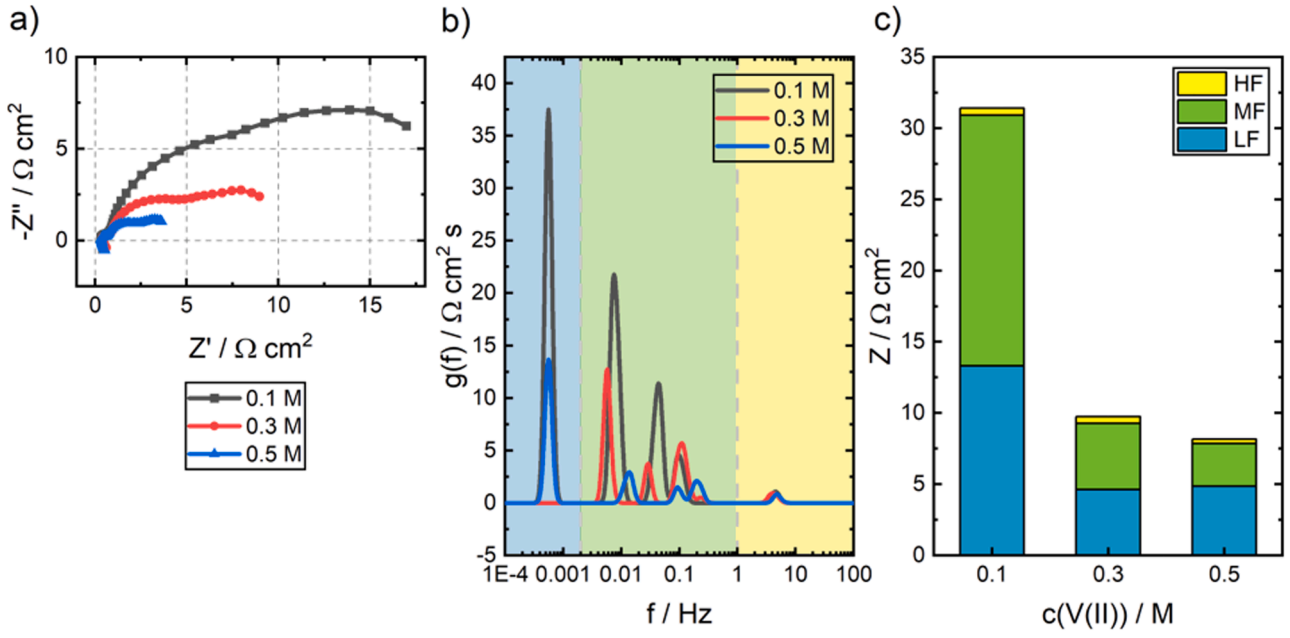

Fig. 5. (a) Nyquist plots and b) corresponding DRT spectra at different V(II) concentrations of 0.1 M, 0.3 M, and 0.5 M V(II) in 2 M H_2SO_4 using carbon paper as the WE. (c) Total impedance values contributing to the assigned frequency ranges.

proposed [15–22]. Yet, the exact reaction mechanism is unknown. Overall, all processes in the negative half-cell improved at higher concentrations, indicating that VRFB operation at high concentrations is beneficial.

3.5. Influence of the temperature

Since the temperature influences the impedance of cell processes, it is crucial to select a suitable operating temperature for high VRFB efficiency [43,44]. Fig. 6 displays the Nyquist plots, DRT spectra, and bar diagrams of EIS measurements at different temperatures. During this study, the temperature was increased from room temperature (20 °C) to 30 °C and 40 °C. In the LF and the MF range, the impedances related to the transport processes decrease with rising temperature since a higher temperature decreases the viscosity of the electrolyte [45]. Thus, due to a higher mass diffusivity, the vanadium ions can be transported more quickly through the electrolyte to the active sites. The effect of rising temperature is especially significant for 20 °C to 30 °C. The diffusion coefficient and the ionic mobility of vanadium ions are temperature-dependent [46].

Surprisingly, the effect of the temperature on the electrochemical reaction is negligible (Fig. 6b). We expected that a temperature variation would influence the electrochemical reaction due to a change in the rate constant, which is usually temperature-dependent. However, the rate-determining step of the V(II)/V(III) reaction seems unaffected, or the temperature change from 20 °C to 40 °C is too tiny to observe a significant difference.

3.6. Influence of the applied potential

This section will display and discuss the influence of the applied WE potential on the impedance data (Fig. 7). A fully charged V(II) electrolyte was used, and different WE potentials were applied between −0.30 V vs. RHE and −0.26 V vs. RHE. These potentials were chosen to ensure the same electrochemical reaction occurs in all experiments. Since the open circuit potential of the solution is larger than −0.30 V vs. RHE, it is guaranteed that only the V(II) oxidation to V(III) occurs since the reaction equilibrium is shifted in this direction.

The Nyquist plot reveals minor differences in the lower frequency, which the DRT analysis can quantify. In the HF range, the single peak is unaffected by changing the applied potential. The HF impedance and the peak position remain similar, which supports the idea that only the V(II) oxidation occurs in the setup. The LF and MF impedances are affected by the change in applied potential. However, compared to the positive half-cell [27], the effect in the negative half-cell is relatively small. A more positive WE potential decreases the impedance of the MF range. If the applied potential is varied, the double layer at the electrode's surface is altered, and the electrostatic force of the electrode is changed. Thus, the concentration of vanadium ions close to the surface varies, and the diffusion and migration of the ions through the electrolyte are influenced. The oxidation of V(II) is favored; thus, the impedance decreases by applying a more positive potential.

3.7. Influence of the SOC

This final section investigated the influence of the electrolyte's SoC (Fig. 8). The same potential of −0.20 V vs. RHE was applied during the EIS measurement to ensure that the same electrochemical reaction, the oxidation from V(II) to V(III), occurs in all measurements.

The HF peak related to the electrochemical reaction remains unaffected by the SoC, proving that the same electrochemical reaction is triggered. Due to the scale of the y-axis, the HF peak is relatively small and cannot be distinguished in the DRT spectra and the bar diagram. In comparison, the peak related to the ion transport in the LF range changes significantly with the SoC. The impedance associated with this process decreases if more V(II) reactant is available, which can undergo the favored oxidation reaction to V(III). For example, fewer V(II) ions that can undergo the oxidation reaction are available in an electrolyte with 25 % SoC compared to the electrolyte with 75 % SoC. Thus, the mean diffusion pathway is more prominent, leading to a higher impedance of the transport process.

4. Conclusion

In this study, the reaction and processes in the negative half-cell of a VRFB were investigated using EIS combined with DRT analysis. Several parameters, including the WE material, the flow rate, the V(II) concentration, the temperature, the applied WE potential, and the SoC of

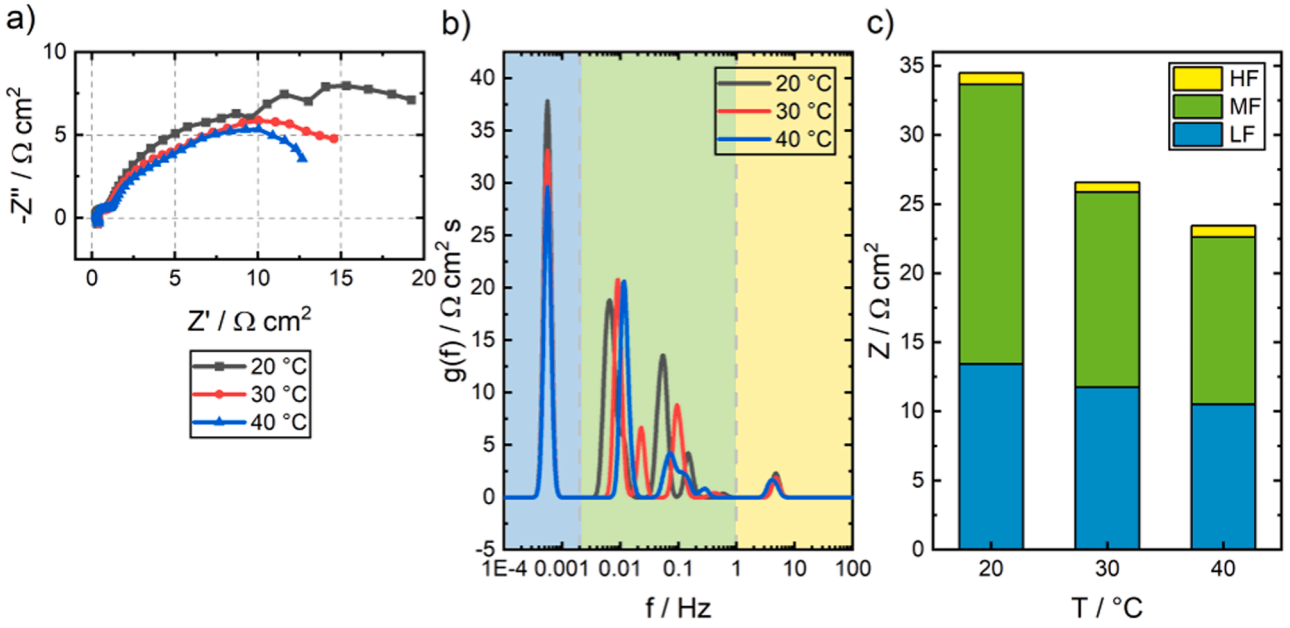

Fig. 6. (a) Nyquist plots and (b) corresponding DRT spectra at different temperatures of 20, 30, and 40 °C using carbon paper as the WE. (c) Total impedance values contributing to the assigned frequency ranges.

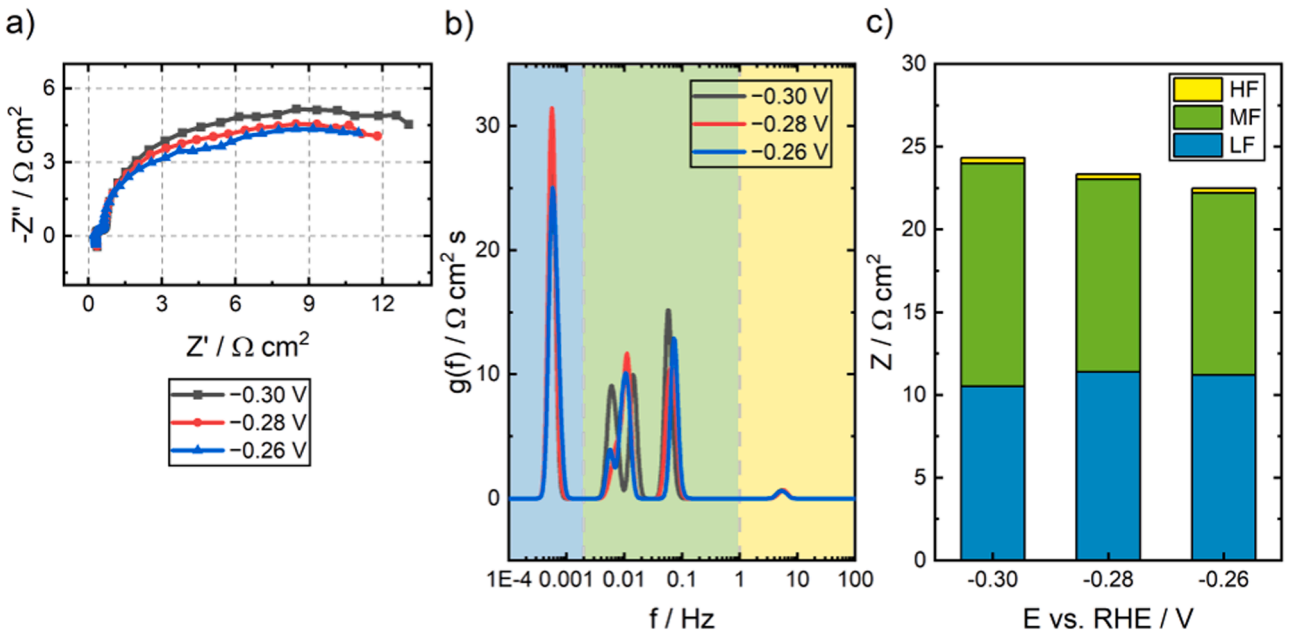

Fig. 7. (a) Nyquist plots and (b) corresponding DRT spectra at different applied potentials of −0.26, −0.28, and −0.30 V vs. RHE using carbon paper as the WE. (c) Total impedance values in the assigned frequency ranges.

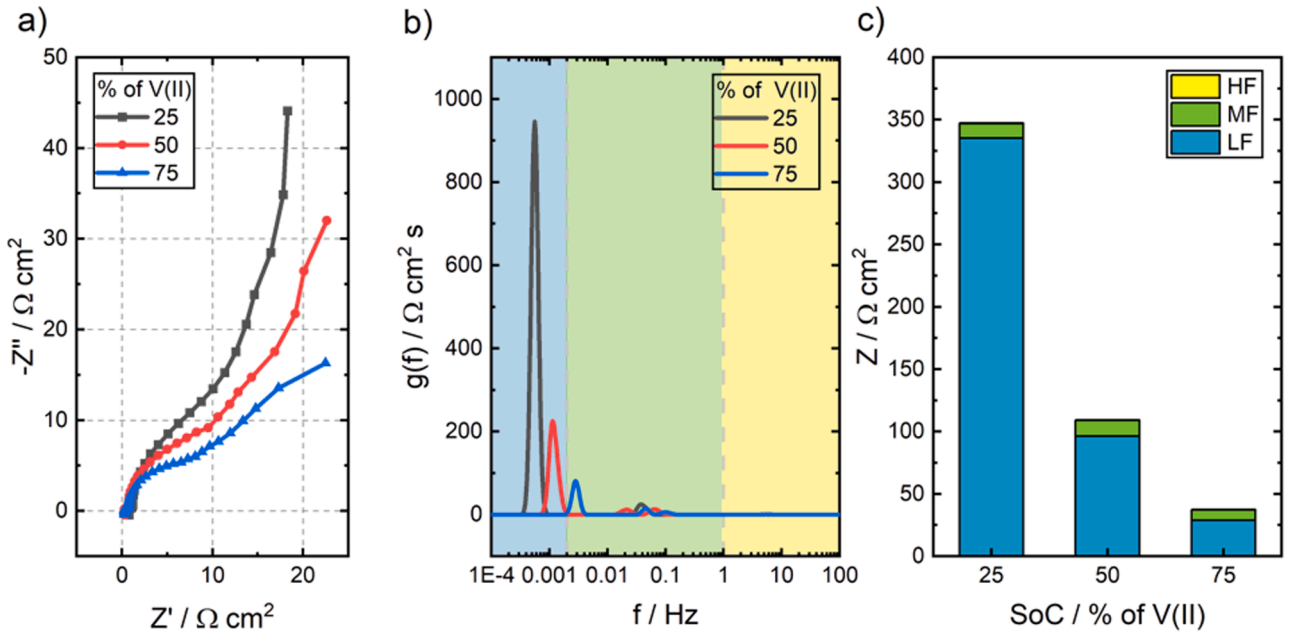

Fig. 8. (a) Nyquist plots and (b) corresponding DRT spectra at different SoCs of 25 %, 50 %, and 75 % using carbon paper as the WE. (c) Total impedance values in the assigned frequency ranges.

the electrolyte, were varied, and the effects on the processes' impedances were studied. We separated and identified the individual processes contributing to the overall impedance in the negative half-cell. The DRT is a valuable tool in separating the superimposed semicircles in the EIS spectrum. Three frequency ranges related to different processes were identified for the negative half-cell. One peak is observed in the LF range below 2 mHz, attributed to the ion transport. Several peaks are identified from 2 mHz to 1 Hz (MF range), assigned to the redox-active species' transport processes through the electrode's porous structure. The knowledge derived from the LF and MF range can help to study the phenomena in novel electrode materials and optimize their structure concerning the impedance of the individual processes. In the HF range above 1 Hz, the single peak was related to the electrochemical reaction in the negative half-cell. The DRT analysis further revealed information about the V(II)/V(III) reaction pathway, hinting that the rate-determining step is influenced by diffusion. For the competing HER, no peak was found in the DRT spectrum.

The results of this work serve as a foundation for developing new EIS equivalent circuits and simulation models of the negative VRFB half-cell. This work presents the second part of studying processes and reactions with EIS and DRT analysis in VRFBs. The results of investigating the positive half-cell were published previously [27]. Additionally, this study demonstrates that operating a VRFB with a high vanadium ion concentration in the electrolyte at elevated temperatures and the

appropriate flow rate improves cell efficiency by reducing impedance losses.

CRediT authorship contribution statement

Monja Schilling: Data curation, Formal analysis, Investigation, Methodology, Visualization, Writing – original draft. **Roswitha Zeis:** Conceptualization, Funding acquisition, Project administration, Supervision, Writing – review & editing.

Declaration of competing interest

The authors declare that they have no known competing financial interests or personal relationships that could have appeared to influence the work reported in this paper.

Data availability

Data will be made available on request.

Acknowledgments

We especially thank SGL Carbon for supplying the SIGRACELL® carbon felt and the SIGRACET® carbon paper. M.S. gratefully acknowledges financial support through a Kekulé Ph.D. fellowship by the Fonds der Chemischen Industrie (FCI). This work contributes to the research performed at CELEST (Center for Electrochemical Energy Storage Ulm-Karlsruhe).

Supplementary materials

Supplementary material associated with this article can be found, in the online version, at doi:10.1016/j.electacta.2024.143771.

References

[1] M. Skyllas-Kazacos, M. Rychcik, R.G. Robins, A.G. Fane, M.A. Green, New all-vanadium redox flow cell, J. Electrochem. Soc. 133 (1986) 1057–1058, https://doi.org/10.1149/1.2108706.
[2] K. Lourenssen, J. Williams, F. Ahmadpour, R. Clemmer, S. Tasnim, Vanadium redox flow batteries: a comprehensive review, J. Energy Storage 25 (2019) 100844, https://doi.org/10.1016/j.est.2019.100844.
[3] N. Bevilacqua, L. Eifert, R. Banerjee, K. Köble, T. Faragó, M. Zuber, A. Bazylak, R. Zeis, Visualization of electrolyte flow in vanadium redox flow batteries using synchrotron X-ray radiography and tomography – impact of electrolyte species and electrode compression, J. Power Sources 439 (2019) 227071, https://doi.org/10.1016/j.jpowsour.2019.227071.
[4] K. Köble, L. Eifert, N. Bevilacqua, K.F. Fahy, A. Bazylak, R. Zeis, Synchrotron X-ray radiography of vanadium redox flow batteries – time and spatial resolved electrolyte flow in porous carbon electrodes, J. Power Sources 492 (2021) 229660, https://doi.org/10.1016/j.jpowsour.2021.229660.
[5] L. Eifert, R. Banerjee, Z. Jusys, R. Zeis, Characterization of carbon felt electrodes for vanadium redox flow batteries: impact of treatment methods, J. Electrochem. Soc. 165 (2018) A2577–A2586, https://doi.org/10.1149/2.0531811jes.
[6] K. Köble, M. Jaugstetter, M. Schilling, M. Braig, T. Diemant, K. Tschulik, R. Zeis, Multimodal characterization of carbon electrodes' thermal activation for vanadium redox flow batteries, J. Power Sources 569 (2023) 233010, https://doi.org/10.1016/j.jpowsour.2023.233010.
[7] M. Cecchetti, M. Messaggi, A. Donazzi, A. Facibeni, V. Russo, C.S. Casari, A. L. Bassi, A. Casalegno, M. Zago, A combined morphological and electrochemical characterization of carbon electrodes in vanadium redox flow batteries: insights into positive and negative electrode performance, Electrochim. Acta 329 (2020) 135143, https://doi.org/10.1016/j.electacta.2019.135143.
[8] I. Derr, D. Przyrembel, J. Schweer, A. Fetyan, J. Langner, J. Melke, M. Weinelt, C. Roth, Electroless chemical aging of carbon felt electrodes for the all-vanadium redox flow battery (VRFB) investigated by Electrochemical Impedance and X-ray Photoelectron Spectroscopy, Electrochim. Acta 246 (2017) 783–793, https://doi.org/10.1016/j.electacta.2017.06.050.
[9] M. Skyllas-Kazacos, L. Cao, M. Kazacos, N. Kausar, A. Mousa, Vanadium electrolyte studies for the vanadium redox battery-a review, ChemSusChem 9 (2016) 1521–1543, https://doi.org/10.1002/cssc.201600102.
[10] T. Lemmermann, M. Becker, M. Stehle, M. Drache, S. Beuermann, M.S. Bogar, U. Gohs, U.E. Fittschen, T. Turek, U. Kunz, *In situ* and in operando detection of redox reactions with integrated potential probes during vanadium transport in ion exchange membranes, J. Power Sources 533 (2022) 231343, https://doi.org/10.1016/j.jpowsour.2022.231343.
[11] L. Eifert, Z. Jusys, R.J. Behm, R. Zeis, Side reactions and stability of pretreated carbon felt electrodes for vanadium redox flow batteries: a DEMS study, Carbon N Y 158 (2020) 580–587, https://doi.org/10.1016/j.carbon.2019.11.029.
[12] L. Eifert, Z. Jusys, R. Banerjee, R.J. Behm, R. Zeis, Differential electrochemical mass spectrometry of carbon felt electrodes for vanadium redox flow batteries, ACS Appl. Energy Mater 1 (2018) 6714–6718, https://doi.org/10.1021/acsaem.8b01550.
[13] C.N. Sun, F.M. Delnick, L. Baggetto, G.M. Veith, T.A. Zawodzinski, Hydrogen evolution at the negative electrode of the all-vanadium redox flow batteries, J. Power Sources 248 (2014) 560–564, https://doi.org/10.1016/j.jpowsour.2013.09.125.
[14] L. Wei, T.S. Zhao, Q. Xu, X.L. Zhou, Z.H. Zhang, In-situ investigation of hydrogen evolution behavior in vanadium redox flow batteries, Appl. Energy 190 (2017) 1112–1118, https://doi.org/10.1016/j.apenergy.2017.01.039.
[15] B. Sun, M. Skyllas-Kazacos, Chemical modification of graphite electrode materials for vanadium redox flow battery application—part II. Acid treatments, Electrochim. Acta 37 (1992) 2459–2465, https://doi.org/10.1016/0013-4686(92)87084-D.
[16] H. Agarwal, J. Florian, B.R. Goldsmith, N. Singh, V 2+ /V 3+ redox kinetics on glassy carbon in acidic electrolytes for vanadium redox flow batteries, ACS Energy Lett. 4 (2019) 2368–2377, https://doi.org/10.1021/acsenergylett.9b01423.
[17] A. Bourke, M.A. Miller, R.P. Lynch, J.S. Wainright, R.F. Savinell, D.N. Buckley, Electrode kinetics in All-vanadium flow batteries: effects of electrochemical treatment, ECS Trans. 66 (2015) 181–211, https://doi.org/10.1149/06608.0181ecst.
[18] T. Greese, G. Reichenauer, Anode kinetics degradation in vanadium redox flow batteries – reversible inhibition of the V2+/V3+-reaction due to V(II)-adsorption, J. Power Sources 500 (2021) 229958, https://doi.org/10.1016/j.jpowsour.2021.229958.
[19] P. Han, H. Wang, Z. Liu, X. Chen, W. Ma, J. Yao, Y. Zhu, G. Cui, Graphene oxide nanoplatelets as excellent electrochemical active materials for VO2+/VO2+ and V2+/V3+ redox couples for a vanadium redox flow battery, Carbon N Y 49 (2011) 693–700, https://doi.org/10.1016/j.carbon.2010.10.022.
[20] W. Li, J. Liu, C. Yan, Graphite–graphite oxide composite electrode for vanadium redox flow battery, Electrochim. Acta 56 (2011) 5290–5294, https://doi.org/10.1016/j.electacta.2011.02.083.
[21] K.J. Kim, M.S. Park, Y.J. Kim, J.H. Kim, S.X. Dou, M. Skyllas-Kazacos, A technology review of electrodes and reaction mechanisms in vanadium redox flow batteries, J. Mater. Chem. A 3 (2015) 16913–16933, https://doi.org/10.1039/C5TA02613J.
[22] X.W. Wu, T. Yamamura, S. Ohta, Q.X. Zhang, F.C. Lv, C.M. Liu, K. Shirasaki, I. Satoh, T. Shikama, D. Lu, S.Q. Liu, Acceleration of the redox kinetics of VO2+/VO2 + and V3+/V2+ couples on carbon paper, J. Appl. Electrochem. 41 (2011) 1183–1190, https://doi.org/10.1007/s10800-011-0343-7.
[23] V.F. Lvovich, Impedance Spectroscopy: Applications to Electrochemical and Dielectric Phenomena, Wiley, Hoboken, N.J, 2012.
[24] M.A. Danzer, Generalized distribution of relaxation times analysis for the characterization of impedance spectra, Batteries 5 (2019) 53, https://doi.org/10.3390/batteries5030053.
[25] A. Weiß, S. Schindler, S. Galbiati, M.A. Danzer, R. Zeis, Distribution of relaxation times analysis of high-temperature PEM fuel cell impedance spectra, Electrochim. Acta 230 (2017) 391–398, https://doi.org/10.1016/j.electacta.2017.02.011.
[26] M.E. Orazem, B. Tribollet, Electrochemical Impedance Spectroscopy, 2nd ed., John Wiley & Sons Inc, Hoboken, New Jersey, 2017.
[27] M. Schilling, M. Braig, K. Köble, R. Zeis, Investigating the V(IV)/V(V) electrode reaction in a vanadium redox flow battery – a distribution of relaxation times analysis, Electrochim. Acta 430 (2022) 141058, https://doi.org/10.1016/j.electacta.2022.141058.
[28] M. Zago, A. Casalegno, Physically-based impedance modeling of the negative electrode in all-vanadium redox flow batteries: insight into mass transport issues, Electrochim. Acta 248 (2017) 505–517, https://doi.org/10.1016/j.electacta.2017.07.166.
[29] Y. Jiang, G. Cheng, Y. Li, Z. He, J. Zhu, W. Meng, L. Dai, L. Wang, Promoting vanadium redox flow battery performance by ultra-uniform ZrO2@C from metal-organic framework, Chem. Eng. J. 415 (2021) 129014, https://doi.org/10.1016/j.cej.2021.129014.
[30] Q. Jiang, Y. Ren, Y. Yang, H. Liu, L. Wang, J. Li, L. Dai, Z. He, High-activity and stability graphite felt supported by Fe, N, S co-doped carbon nanofibers derived from bimetal-organic framework for vanadium redox flow battery, Chem. Eng. J. 460 (2023) 141751, https://doi.org/10.1016/j.cej.2023.141751.
[31] M. Braig, R. Zeis, Distribution of relaxation times analysis of electrochemical hydrogen pump impedance spectra, J. Power Sources 576 (2023) 233203, https://doi.org/10.1016/j.jpowsour.2023.233203.
[32] K. Köble, A. Ershov, K. Duan, M. Schilling, A. Rampf, A. Cecilia, T. Faragó, M. Zuber, T. Baumbach, R. Zeis, Insights into the hydrogen evolution reaction in vanadium redox flow batteries: a synchrotron radiation based X-ray imaging study, J. Energy Chem. (2023), https://doi.org/10.1016/j.jechem.2023.12.010.
[33] M. Schilling, L. Eifert, K. Köble, M. Jaugstetter, N. Bevilacqua, K.F. Fahy, K. Tschulik, A. Bazylak, R. Zeis, Investigating the influence of treatments on carbon felts for vanadium redox flow batteries, ChemSusChem 17 (1) (2024) e202301063, https://doi.org/10.1002/cssc.202301063.
[34] A.M. Pezeshki, J.T. Clement, G.M. Veith, T.A. Zawodzinski, M.M. Mench, High performance electrodes in vanadium redox flow batteries through oxygen-enriched thermal activation, J. Power Sources 294 (2015) 333–338, https://doi.org/10.1016/j.jpowsour.2015.05.118.

[35] M. Schönleber, E. Ivers-Tiffée, Approximability of impedance spectra by RC elements and implications for impedance analysis, Electrochem. Commun. 58 (2015) 15–19, https://doi.org/10.1016/j.elecom.2015.05.018.
[36] M. Schönleber, D. Klotz, E. Ivers-Tiffée, A method for improving the robustness of linear kramers-kronig validity tests, Electrochim. Acta 131 (2014) 20–27, https://doi.org/10.1016/j.electacta.2014.01.034.
[37] T.H. Wan, M. Saccoccio, C. Chen, F. Ciucci, Influence of the discretization methods on the distribution of relaxation times deconvolution: implementing radial basis functions with DRTtools, Electrochim. Acta 184 (2015) 483–499, https://doi.org/10.1016/j.electacta.2015.09.097.
[38] SGL CARBON GmbH, SIGRACELL battery felts - Datasheet (www.sigracell.com), 2019.
[39] H. Kim, Y.J. Lee, D.C. Lee, G.G. Park, Y. Yoo, Fabrication of the carbon paper by wet-laying of ozone-treated carbon fibers with hydrophilic functional groups, Carbon N Y 60 (2013) 429–436, https://doi.org/10.1016/j.carbon.2013.04.057.
[40] R. Schweiss, C. Meiser, T. Damjanovic, I. Galbati, N. Haak 2023 SIGRACET gas diffusion layers for PEM fuel cells, electrolyzers and batteries: white paper.
[41] R. Schweiss, S. Hofmeister, C. Meiser, D. Dan, A. Baumann, T. Kuster, N. Haak, S. Bacher, Powering up fuel cells: our gas diffusion layer (White Paper), 2021.
[42] F. Rahman, M. Skyllas-Kazacos, Vanadium redox battery: positive half-cell electrolyte studies, J. Power Sources 189 (2009) 1212–1219, https://doi.org/10.1016/j.jpowsour.2008.12.113.
[43] C. Zhang, T.S. Zhao, Q. Xu, L. An, G. Zhao, Effects of operating temperature on the performance of vanadium redox flow batteries, Appl. Energy 155 (2015) 349–353, https://doi.org/10.1016/j.apenergy.2015.06.002.
[44] R. Schweiss, C. Meiser, D. Dan, Effect of operating temperature on individual half-cell reactions in all-vanadium redox flow batteries, Batteries 4 (2018) 55, https://doi.org/10.3390/batteries4040055.
[45] X. Li, J. Xiong, A. Tang, Y. Qin, J. Liu, C. Yan, Investigation of the use of electrolyte viscosity for online state-of-charge monitoring design in vanadium redox flow battery, Appl. Energy 211 (2018) 1050–1059, https://doi.org/10.1016/j.apenergy.2017.12.009.
[46] S. Yin, L. Zhou, X. Du, Y. Yang, Influence of temperature on performance of all vanadium redox flow battery: analysis of ionic mass transfer, Ionics 25 (2019) 593–606, https://doi.org/10.1007/s11581-018-2626-z. Kiel.